

# Remarks on the Proton Structure

E. Comay\*  
Charactell Ltd.  
PO Box 39019  
Tel-Aviv 61390, Israel

Elastic and inelastic cross sections of proton-proton and electron-proton scattering are discussed. Special attention is given to elastic scattering and to the striking difference between the data of these two kinds of experiments. It is shown that the regular charge-monopole theory explains the main features of the data. Predictions of results of CERN's Large Hadron Collider are pointed out.

*Keywords:* Proton Structure, Magnetic Monopole, Scattering Data

## 1. Introduction

Scattering experiments are used as a primary tool for investigating the structure of physical objects. These experiments can be divided into several classes, depending on the kind of colliding particles. The energy involved in scattering experiments has increased dramatically during the previous century since the cel-

ebrated Rutherford experiment was carried out (1909). Now, the meaningful value of scattering energy is the quantity measured in the rest frame of the projectile-target center of energy. Therefore, devices that use colliding beams enable measurements of very high energy processes. The new Large Hadron Collider (LHC) facility at CERN, which is designed to produce 14 TeV proton-proton ( $pp$ ) collisions, will make a great leap forward.

This work examines two different scattering data of protons. One set consists of the pre-LHC  $pp$  scattering data and the second set is electron-proton and positron-proton scattering data. Hereafter,  $ep$  denote these lepton-proton scattering experiments. Special attention is given to elastic scattering (ES), where the proton remains intact and no new particle is produced. The data prove that the elastic cross section (ECS) of  $pp$  scattering differs dramatically from that of  $ep$ . These experimental data are explained by the Regular Charge-Monopole Theory (RCMT). It is also shown how this theory together with currently available data yields a prediction of the LHC results.

The Lorentz metric used is diagonal and its entries are (1,-1,-1,-1). Expressions are written in units where  $\hbar = c = 1$ . In this system of units there is just one dimension. Here it is taken to be that of length. Therefore, the dimension of a physical quantity is a power of length and is denoted by  $[L^n]$ .

The data on cross sections of  $pp$  and  $ep$  are presented in the second section. An analysis of these data and a theoretical explanation of their main features are included in the third section. The fourth section discusses the structure of the baryonic core. The last section contains concluding remarks.

## 2. The Relevant Cross-Section Data

Let us turn to the  $pp$  scattering (see fig. 1 and its original version [1]). Points  $A$ ,  $B$ ,  $C$  divide the ECS graph into four parts. For a laboratory momentum smaller than that of point  $A$ , the elastic cross section shows the characteristic decreasing pattern of a Mott-like scattering.

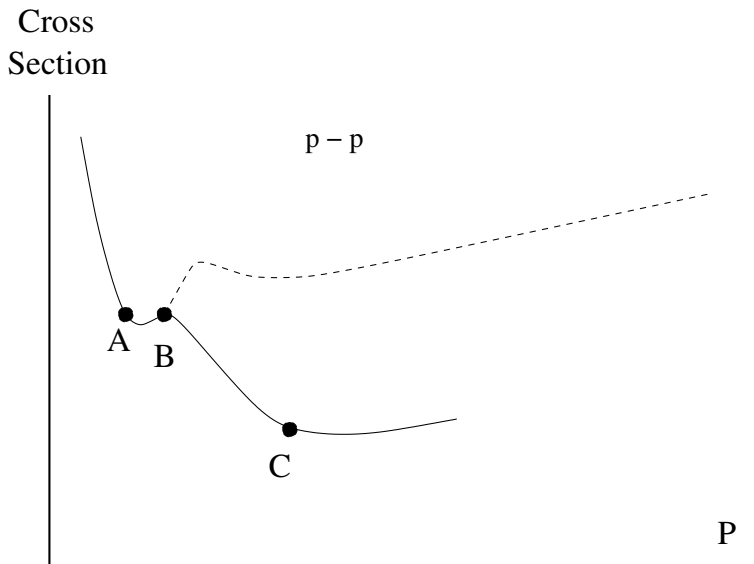


Figure 1: *The pre-LHC Proton-proton cross section versus the laboratory momentum  $P$ . Axes are drawn in a logarithmic scale. The continuous line denotes the elastic cross section and the broken line denotes the total cross section. Points  $A, B, C$  will facilitate the discussion (see text). (The accurate figure can be found in [1]).*

Clearly, the Mott-like decrease of the cross section does not hold for a momentum greater than that of point  $A$ . For the momentum interval  $[A, B]$ , a new force enters the scattering process. This is the nuclear force whose phenomenological properties have long been well known [2]. Its main features are a quite strong repulsive force at the nucleon's inner part and an attractive force outside it. The nuclear attractive force decays more rapidly than the Coulomb force. At a short distance from the proton's center, these forces are much stronger than the electromagnetic force. (The fact that near the origin the potential of the nuclear force  $V(r)$  varies more rapidly than the potential of the Coulomb force  $1/r$  is significant. This point is discussed in the third section.) For momentum values belonging to the interval  $[A, B]$ , the nuclear force alters the direction of the ECS graph. Here the ECS decrease disappears and at a certain interval of the projectile's momentum, the ECS increases with it.

Let us examine the momentum interval belonging to points  $[B, C]$ . Fig. 1 indicates that a new process begins to take place for momentum values greater than that of point  $B$ . For these values, the collision's energy is high enough for the production of hadrons. It means that inelastic scattering begins at point  $B$ . The inelastic cross section (ICS) is the difference between the broken line describing the total cross section (TCS) and the continuous line describing the ECS. Thus, for momentum values greater than that of point  $B$ , the ECS begins to decrease. An examination of the scale of the original figure [1] indicates that the ICS becomes greater than ECS and at point  $C$ , the ICS is about five times greater than the ECS.

For momentum values greater than that of point  $C$ , the decreasing pattern of the ECS gradually stops and it slightly begins

to increase together with the momentum. It can be concluded that points  $A, B, C$  of the graph show clearly four momentum regions, each of which has a unique behavior of the ECS.

In the second kind of scattering data, one proton is replaced by an electron. Unfortunately, publications of the Particle Data Group do not contain an  $ep$  cross-section figure which is analogous to fig. 1. Therefore, the discussion relies on appropriate formulas that describe the data. The following arguments prove that in  $ep$  scattering, the characteristics of the cross section differ substantially from the  $pp$  data depicted in fig. 1.

Let us examine the elastic  $ep$  scattering. In this case the analysis uses the Rosenbluth formula. Here the Mott cross section is factored out and is multiplied by trigonometric functions and form factors which depend on the square of the 4-momentum transferred  $q^2$ . The Mott differential cross section takes the following form (see [3], p. 192)

$$\left(\frac{d\sigma}{d\Omega}\right)_{Mott} = \frac{\alpha^2 \cos^2(\theta/2)}{4p^2 \sin^4(\theta/2)[1 + (2p/M) \sin^2(\theta/2)]}, \quad (1)$$

where  $\alpha \simeq 1/137$  denotes the square of the electron's charge and  $p$  is the linear momentum of the incoming electron. The Rosenbluth formula can be cast into the following form (see [3], p. 193, eq. (6.26))

$$\left(\frac{d\sigma}{d\Omega}\right)_{Rosenbluth} = \left(\frac{d\sigma}{d\Omega}\right)_{Mott}(A(q^2) + B(q^2) \tan^2(\theta/2)), \quad (2)$$

where  $A$  and  $B$  are related to the proton's electric and magnetic form factors.

In the  $ep$  case, the Rosenbluth formula (2) is used for describing ECS. This formula is valid even for the very high energy of

modern colliders [4]. A useful quantity is called the dipole form factor (see [3], p. 196)

$$G_D(q^2) = (1 + q^2/0.71)^{-2}, \quad (3)$$

where  $q^2$  is measured in  $\text{GeV}^2$ . It turns out that, for all energies used to date, the actual form factors are nearly the same as (3). For the present discussion it is sufficient to realize that the actual form factors are of the same order of magnitude as (3) (see figures 2, 3 of [5]). It can be concluded that the  $ep$  elastic form factor decreases with an increase of  $q^2$  and for  $q^2 \gg 1 \text{ GeV}^2$ , the contribution of the electric form factor  $G_E$  decreases like  $q^{-4}$  and that of the magnetic form factor decreases like  $q^{-2}$  (see [3], p. 193). Moreover, these decreasing contributions are multiplied by the Mott cross section that decreases like  $p^{-2}$ .

The form of the deep inelastic cross section is quite different. Using the notation of [3], sections 8.2 and 8.3, one finds for deep inelastic collisions

$$\left(\frac{d^2\sigma}{dq^2 dx}\right) = \frac{4\pi\alpha^2}{q^4} \left[ (1-y) \frac{F_2(x, q^2)}{x} + y^2 F_1(x, q^2) \right]. \quad (4)$$

Here  $x$  and  $y$  are dimensionless variables whose value falls in the range  $[0,1]$ . Experimental evidence proves that Bjorken scaling holds and that the expression inside the square brackets of (4) is very nearly independent of  $q^2$ . Hence, integrating (4) on  $q^2$ , one finds that the deep inelastic cross section decreases like  $1/q^2$ . This is the rate of the decrease of the magnetic form factor contribution to the elastic scattering.

The first interesting issue is the ratio of the ECS to the TCS which is found for very high energy. As stated above, in the case

of  $pp$  scattering, this ratio is about  $1/6$ . On the other hand, the additional  $1/p^2$  factor of the Mott cross section (1) proves that in  $ep$  scattering, elastic events are very rare. Hence, the data lead one to the following conclusion:

- I. For very high energy, about 16% of the  $pp$  scattering events are elastic whereas in the corresponding  $ep$  scattering, the percentage of elastic events is very, very low.

The second issue is the behavior of the ECS as a function of energy in the two kinds of scattering experiments described above. The data of fig. 1 (see [1]) shows how the  $pp$  cross section varies as a function of either the projectile's momentum or, equivalently, on a different scale, as a function of  $\sqrt{S}$ , where  $S$  is the square of the invariant energy of the colliding particles.

The ECS graph of fig. 1 shows that it stops decreasing for energies which are somewhat greater than that of point  $C$ . In the case of the  $ep$  scattering, the ECS information is given in terms of the differential cross section which depends on the invariant square of the momentum transferred  $q^2$ . However, the following calculation proves that for  $ep$  scattering ECS does not stop decreasing with the increase of the collision's energy.

The calculation is carried out in the rest frame of the colliding particles. Let the 4-momentum of the incoming electron be

$$p_{in}^\mu = (\sqrt{p^2 + m^2}, 0, 0, p) \quad (5)$$

and that of the outgoing electron is

$$p_{out}^\mu = (\sqrt{p^2 + m^2}, p \sin \theta, 0, p \cos \theta). \quad (6)$$

It follows that the square of the momentum transferred is

$$q^2 = (p_{in}^\mu - p_{out}^\mu)(p_{\mu in} - p_{\mu out}) = 2p^2(1 - \cos \theta). \quad (7)$$

Now the elastic cross section  $\sigma$  is the spherical integral of the Rosenbluth differential cross-section formula (2)

$$\sigma = \int \left( \frac{d\sigma}{d\Omega} \right)_{\text{Rosenbluth}} \sin \theta d\theta d\phi. \quad (8)$$

Let us examine the integrand of (8) at a certain value of  $(\theta, \phi)$ . Relation (7) proves that a replacement of  $q^2$  by  $p^2$  is followed by a trigonometric factor. Now if  $p$  increases then the Mott factor (1) decreases and the same is true for the dipole factor (3). Therefore, since the differential cross section is positive and it decreases for all values of  $(\theta, \phi)$ , one concludes that the spherical integral (8) also decreases with increasing momentum. This outcome proves that for the  $ep$  scattering discussed here, the ECS does not stop decreasing with an increase of the linear momentum. The validity of the following conclusion relies on these results.

II. For high enough energy there is a substantial difference between elastic scattering of  $pp$  and of  $ep$ . If the collision energy increases, then the ECS of  $pp$  stops decreasing and even shows a small increase, whereas the ECS of  $ep$  does not stop decreasing.

There is another kind of difference between  $ep$  and  $pp$  scattering. The Mott formula decreases like  $1/p^2$ . This matter is evident on the basis of dimensions arguments. The cross section has the dimension  $[L^2]$ . In the system of units used here, energy and momentum have the dimension  $[L^{-1}]$  and the coupling constant  $\alpha$  is dimensionless. This argument explains the negative slope of the cross section  $\sigma(p^2)$  of the Mott formula (1) and of the deep inelastic scattering of  $ep$  (4).

This property does not hold for the  $pp$  scattering. Here one sees that for low momentum, which is smaller than that of point  $A$  of fig. 1, the TCS decreases steeply, as expected from the Mott formula. Let us turn to momentum values which are greater than that of point  $A$  of fig. 1. For most of these momentum regions, the TCS increases and at a short region of momentum values, it decreases. However, the decrease rate is much smaller than the quite steep slope of  $1/p^2$ . Therefore, it is concluded that

- III. Unlike the case of  $ep$  scattering, one finds that for high enough energy, the TCS of  $pp$  does not follow the  $1/p^2$  decrease of the Mott formula.

Physical consequences of conclusions I-III of this section are discussed in the remainder of this work.

### 3. A Discussion of the Cross Sections

The  $pp$  and  $ep$  scattering experiments help us understand the proton's structure. Conclusions I-III of the previous section reveal a dramatic difference between the results of these experiments. For example, experiments done in the HERA facility at DESY report on  $ep$  collisions where  $q^2 > 10000 \text{ GeV}^2$  [6-8]. Substituting these values of  $q^2$  into the dipole formula (3), and remembering that the magnetic form factor dominates very high  $q^2$  collisions, one finds that for  $ep$  scattering the ratio of the ECS to the ICS is less than  $10^{-4}$ . On the other hand, in the  $pp$  scattering this ratio is about  $1/5$ . Physical aspects of these properties are important for the discussion carried out below. Therefore, they are summarized as follows:

1. For nearly all events of energetic collisions of electrons with

proton quarks, the proton is broken apart and the fragments come out as a set of hadrons. The relative number of elastic collisions where the proton remains intact is very, very small.

2. In a  $pp$  collision of similar energy, about 16% of the events are elastic and in these cases the proton remains intact.

The  $ep$  scattering data teaches us that if a quark is struck violently by a projectile then an inelastic process results (and that the number of elastic events is negligible). Moreover, in this process, the cross section decreases with the increasing momentum of the projectile. Therefore, valence quarks together with the additional  $\bar{q}q$  pairs cannot explain the  $pp$  scattering data.

The following explanation of properties 1,2 is adopted here:

- a. The proton consists of quarks and of another object called the baryonic core. The existence of the baryonic core is consistent with the experimental evidence showing that for an ultra-relativistic proton, quarks carry just about one half of the proton's linear momentum (see [3], p. 282).
- b. The baryonic core is electrically neutral (valence quarks carry the entire proton charge). Therefore, electrons do not interact with it. (Conditions for a possible deviation from this behavior are discussed in the next section.)
- c. The baryonic core participates in strong interactions. Hence, three kinds of interacting pairs of particles exist in a very high energy  $pp$  collision: quark-quark, quark-core and core-core.

- d. The core is a relatively rigid object and a core-core interaction is likely to produce an elastic collision.

Statements a-d make a phenomenological explanation of the data discussed in this work in general and of points 1,2 in particular. Thus, in a  $pp$  collision there is a core-core interaction. The relative rigidity of the core is the primary reason for the non-negligible part of the ECS in a  $pp$  collision. The fact that the core is electrically neutral explains why it does not contribute to the ECS of  $ep$  collisions. The following lines present a theoretical basis for points a-d.

It has been proved that one can use very well established physical principles and construct a regular theory of electric charges and magnetic monopoles of the RCMT [9,10]. The main results of the RCMT can be put in the following words:

Charges do not interact with bound fields of monopoles and monopoles do not interact with bound fields of charges. Charges interact with all fields of charges and with radiation fields emitted from monopoles. Monopoles interact with all fields of monopoles and with radiation fields emitted from charges. Another important result of the RCMT is that the unit of the elementary magnetic charge  $g$  is a free parameter. However, hadronic data indicate that this unit is much larger than that of the electric charge  $g^2 \gg e^2 \simeq 1/137$ . More details of the RCMT can be found in [9-11].

These properties of the RCMT perfectly fit the data of electromagnetic projectiles interacting with nucleons (see [11], pp. 90-92). Thus, protons and neutrons do not look alike in cases of charged lepton scattering, whereas they look very similar if the projectile is a hard enough real photon (see [12] and the figure

on p. 369 of [1]).

Electrodynamics of magnetic monopoles is dual to electrodynamics of electric charges. This analogy is helpful for understanding the applicability of the RCMT to hadrons in general and to baryons in particular. Baryons do not show the static force that should be found between monopoles. Therefore, one must assume that they are neutral with respect to a magnetic charge. Thus, each quark is assumed to carry one negative unit of monopole. The overall monopole charge of baryons vanishes because the baryonic core carries three positive units of magnetic charge. (The relative sign of the monopole charge of quarks and of the baryonic core is arbitrary. Here it is defined so that the similarity with the respective electric charge of electrons and nuclei holds.) The elementary unit of magnetic charge is much larger than that of the electric charge. For this reason, baryonic quarks are very tightly bound to the core (provided the comparison is made with atomic electrons). Therefore, a baryon can be regarded as a magnetic monopole analog of an atom, where quarks are strongly bound to the core. A quark is analogous to an electron and the baryonic core is analogous to the atomic nucleus.

Now let us use this proton's structure together with very well established physical principles for a qualitative interpretation of the  $pp$  elastic scattering data of fig. 1. The discussion is carried out in the rest frame of the center of energy of the  $pp$  system. In this frame, the energy of an elastically scattered proton is the same as that of its initial energy. Therefore, in this case the elastic scattering process can be regarded as a scattering from a phenomenological potential  $V(r)$ .

Let us examine an outgoing proton at an angle of  $\theta$  in the

$(x, z)$  plane. Its 3-momentum transferred is

$$\mathbf{q} = (0, 0, p) - (p \sin \theta, 0, p \cos \theta) = p(-\sin \theta, 0, 1 - \cos \theta) \quad (9)$$

and

$$\mathbf{q} \cdot \mathbf{r} = pr(\cos \theta - 1) = -2pr \sin^2(\theta/2). \quad (10)$$

Another issue is the relationship between the spatial range of a potential and the corresponding proton's wave length that makes a meaningful contribution to the cross section. Thus, let us examine a very energetic projectile. Here the wave length is very short with respect to the linear size of the spatial domain of a smoothly varying potential. Therefore, the rapid change of the wave's sign yields a large cancellation effect and a small contribution to the cross section. Thus, one finds that for every potential there is a meaningful range of wave length where its contribution is significant and that this contribution decreases rapidly for much shorter wave length of the projectile. Several illustrations of this property are described below.

The following relationship is useful for the discussion of the ECS  $pp$  graph of fig. 1. Thus, if the phenomenological potential takes the form of a power

$$V(r) = 1/r^a, \quad (11)$$

then the ECS practically depends on a power of the incoming momentum. Indeed, the scattering matrix is

$$M_{if} = \int e^{i\mathbf{q}\cdot\mathbf{r}} \frac{1}{r^a} r^2 \sin \theta \, dr \, d\theta \, d\phi \quad (12)$$

(see [3], p. 186). Let us define a new integration variable  $s = pr$ . Using (10), one obtains a dependence on a power of the

momentum

$$M_{if} = \frac{1}{p^{3-a}} \int e^{-i2s \sin^2(\theta/2)} \frac{1}{s^{a-2}} \sin \theta \, ds \, d\theta \, d\phi. \quad (13)$$

The final result is obtained from a substitution of both (13) and the density of states into the expression for the cross section.

Thus, in the logarithmic scale of the axes of fig. 1, a potential that phenomenologically takes the form of (11) yields a straight line for the momentum interval where this potential is dominant. The ECS graph of fig. 1 proves that this property holds for momentum values smaller than those of points  $A, C$ , respectively.

The Coulomb potential between the protons' electric charge yields the Rutherford and the Mott (1) scattering formulas, where the cross section decreases like  $1/p^2$ . This argument shows that the linearity of the cross-section graph on the left-hand side of point  $A$  and its slope are consistent with the theory.

Let us turn to the momentum values of the interval  $[A, B]$ . Here the nuclear force enters the process. As is well known, relative to the Coulomb force between charges, this force varies very rapidly at the spatial region where it is not negligible and is much stronger. The nuclear force contains a very strong repulsive component at inner parts of the proton and an attractive force outside it. The attractive force decays much more rapidly than the Coulomb force (see the figure on p. 97 of [13]). This form of the nuclear force and of its potential is very far from the power formula (11). Therefore, the twist of the ECS graph between points  $[A, B]$  is understood.

For momentum values of the interval  $[B, C]$  a similar Coulomb effect is found inside the proton. Indeed, one should remember

that by analogy with electrons in an atom, valence quarks screen the core's magnetic monopole potential. Therefore, as a particle (either a quark or the core of the projectile) approaches the baryonic core of the target, the screening effect reduces and the interaction increases more rapidly than the  $1/r$  rate of a Coulomb potential. (It means that in this region, a phenomenological potential takes the form of  $1/r^b$ , where  $b > 1$ .) Hence, the contribution of the quark-core and core-core interaction increases. The former affects the ICS and the latter affects the ECS. Thus, the linearity of the ECS graph between points  $[B, C]$  is understood, together with its milder decreasing slope (relative to the slope on the left-hand side of point  $A$ ).

The next section contains a discussion of the data on the right-hand side of point  $C$  of fig. 1.

## 4. The Structure of the Baryonic Core

Up to this point, the discussion relies only the fact that the baryonic core carries three units of monopole charge. (This property is mandatory for the RCMT, because of the need to explain the neutrality of baryons with respect to magnetic charge.) Referring to the problem of the core's structure, one may consider two alternatives:

1. The core is a simple elementary pointlike object.
2. The core contains closed shells of quarks.

The first case is certainly simpler than the second. However, one should not expect to find that Nature is overly simple. In particular, there are two different experimental data that support the second case.

Experiments carried out in the HERA facility at DESY [6-8] report that the number of events of very high  $q^2$   $ep$  scattering is more than expected. This result can be explained as an analog of the Franck-Hertz experiment: an energy exchange with bound particles takes place only if the projectile's energy is high enough. In the present discussion, the bound particles are quarks of closed shells of the baryonic core. A different kind of data is the charge radius of the proton and that of the  $\pi^\pm$  meson. It can be shown why these data provide two different arguments supporting the existence of closed shells of quarks at the baryonic core [14]. On the basis of these experiments, it is assumed here that the baryonic core has closed shells of quarks. Let us see how this assumption is related to the data of fig. 1 and how it is expected to affect the results of CERN's LHC.

First, let us examine the data of fig. 1 on the right-hand side of point  $C$ . Like all quarks, quarks of closed shells at the baryonic core satisfy the Pauli exclusion principle. Therefore, their interaction with quarks of the other proton (either valence quarks or quarks of its closed shells) has a strong repulsive component. (This repulsion is analogous to the repulsive component of the nuclear force. The repulsive component of the nuclear force is related to the three valence quarks, whereas this force is related to quarks belonging to the closed shells of the baryonic core. Both forces have the quantum mechanical origin of the Pauli exclusion principle.) This repulsion is added to the magnetic monopole core-core Coulomb repulsion. Therefore, the increase of the interaction reduces the decreasing slope of the graph of the ECS at point  $C$  of fig. 1. It can be said that the increase of the ECS graph on the right-hand side of point  $C$  provides another indication supporting the existence of closed

shells of quarks at the baryonic core.

The HERA experiments also provide information on the energy required for exciting quarks belonging to the baryonic core. This statement relies on [6-8] whose results are explained by this kind of excitation. At HERA, the proton energy is 820 GeV and that of the positron is 27.5 GeV [7]. Obviously, for these ultra-relativistic values, these numbers also represent the linear momentum. At the LHC, a proton replaces HERA's positron. Here a rough comparison of the collision energy of these colliders is described. The evaluation uses an appropriate replacement of the positron, which is an elementary pointlike particle, by one of the protons that participate in the LHC collision. Thus, let  $P$  denote an LHC proton that corresponds to a proton at HERA and  $P'$  denotes an LHC proton that replaces HERA's positron. Now, we know that in an ultra-relativistic proton, valence quarks together with the additional  $\bar{q}q$  pairs carry about one half of the proton's momentum (see [3], p. 282). Hence, all quarks of  $P'$  carry kinetic energy of 3500 GeV and each quark of  $P'$  carries about 800 GeV of kinetic energy. (This estimate relies on the fact that beside the three valence quarks, there is a nonvanishing probability that the proton contains  $\bar{q}q$  pairs.) These arguments show that at the LHC, the energy of the proton  $P$  is more than eight times larger than that of HERA's proton and the energy of each quark of the LHC's  $P'$  is about 30 times larger than that of HERA's positron. It follows that the LHC collisions with the baryonic core will be much more energetic than the HERA collisions.

Relying on this analysis, one can predict that the number of energetic LHC events will be more than those which are expected on the basis of the present knowledge of valence quarks and of

$\bar{q}q$  pairs. Obviously, excited quarks of the core are expected to behave like valence quarks and contribute mainly to an inelastic process. In other words, for this gigantic energy, the baryonic core stops behaving as a rigid object. These arguments lead to the following predictions of the LHC results:

1. For very energetic LHC collisions, more inelastic events will be found (comparing to the collider's data of [1]).
2. This increase in the number of inelastic events will probably be accompanied by a *decrease* in the number of elastic events.

## 5. Conclusions

This work discusses the striking difference between high energy  $ep$  scattering and  $pp$  scattering data. Elastic events are very, very rare in high energy  $ep$  scattering. Therefore it is concluded that if a valence quark (or a member of a  $\bar{q}q$  pair) is hit by an energetic projectile then an inelastic event follows.

In the corresponding  $pp$  scattering, elastic events are about 1/5 of the number of inelastic events. Hence, the relative portion of elastic events is larger by several orders of magnitude than that of the corresponding events of  $ep$  scattering. Therefore, one must look for another component included in the proton. This component must be rigid enough to absorb the energy exchanged in a high energy collision without causing a proton to disintegrate into a set of hadrons. Since this component is not detected by electrons (and not by positrons), it must be electrically neutral. This proton component is called here the baryonic core.

The existence of a baryonic core is a self-evident result of the Regular Charge-Monopole Theory. Therefore, the experimental data discussed in this work provide another support for the applicability of this theory to hadrons. (See [11] for other arguments of this kind.)

It is also explained why one should expect the baryonic core to contain closed shells of quarks. The HERA data indicate that the LHC energy is higher than the energy required for exciting quarks of the baryonic core. Therefore, the first prediction made at the end of the previous section says that the very energetic collisions of the LHC will produce more inelastic events than expected on the basis of present collider data of valence quarks. A support for this prediction can be found in the highest part of [1], which is based on cosmic ray experiments. A second prediction says that the increase in the number of inelastic events will be followed by a decrease in the number of elastic events. An LHC confirmation of these predictions will provide another support for the relevance of the Regular Charge-Monopole Theory to strong interactions.

It is interesting to note that the contemporary literature does not contain an adequate theoretical discussion of the pre-LHC  $pp$  scattering data of fig. 1. Moreover, the inconsistency of QCD with these data has already been pointed out in the literature [15].

## References

- \* Email: [elicomay@post.tau.ac.il](mailto:elicomay@post.tau.ac.il)  
Internet site: <http://www.tau.ac.il/~elicomay>
- [1] C. Amsler et al., Phys. Lett. B **667**, 1 (2008). (See p. 364).
- [2] A. deShalit and H. Feshbach, *Theoretical Nuclear Physics* (John Wiley, New York, 1974). Vol 1, pp. 11-18.
- [3] D. H. Perkins, *Introduction to High Energy Physics* (Addison-Wesley, Menlo Park CA, 1987).
- [4] I. A. Qattan et al., Phys. Rev. Lett., **94**, 142301 (2005).
- [5] H. Gao, Int. J. Mod. Phys. E **12**, 1 (2003).
- [6] C. Adloff et al. *Z. Phys. C* **74**, 191 (1997).
- [7] J. Breitweg et al. *Z. Phys. C* **74**, 207 (1997).
- [8] A. Wagner *Tr. J. of Physics* **22** 525 (1998).
- [9] E. Comay *Nuovo Cimento B* **80**, 159 (1984).
- [10] E. Comay *Nuovo Cimento B* **110**, 1347 (1995).
- [11] E. Comay *A Regular Theory of Magnetic Monopoles and Its Implications in Has the Last Word Been Said on Classical Electrodynamics?* ed. A. Chubykalo, V. Onoochin, A. Espinoza and R. Smirnov-Rueda (Rinton Press, Paramus, NJ, 2004).
- [12] T. H. Bauer, R. D. Spital, D. R. Yennie and F. M. Pipkin *Rev. Mod. Phys.* **50**, 261 (1978).

- [13] S. S. M. Wong, *Introductory Nuclear Physics* (Wiley, New York, 1998).
- [14] E. Comay, <http://www.tau.ac.il/~elicomay/LHC.pdf>
- [15] A. A. Arkhipov, [http://arxiv.org/PS\\_cache/hep-ph/pdf/9911/9911533v2](http://arxiv.org/PS_cache/hep-ph/pdf/9911/9911533v2)